

## Interplay between dislocation type and local structure in dislocation-twin boundary reactions in Cu

Khanh Dang <sup>1,\*</sup>, Avnish Mishra,<sup>2</sup> Sumit Suresh <sup>3</sup>, Nithin Mathew <sup>2</sup>, Edward M. Kober,<sup>2</sup> and Saryu Fensin <sup>3,\*</sup><sup>1</sup>MST-8, Los Alamos National Laboratory, Los Alamos, New Mexico 87544, USA<sup>2</sup>T-1, Los Alamos National Laboratory, Los Alamos, New Mexico 87544, USA<sup>3</sup>MPA-CINT, Los Alamos National Laboratory, Los Alamos, New Mexico 87544, USA

(Received 28 November 2023; accepted 30 May 2024; published 20 June 2024)

Dislocation-twin boundary interactions in Cu are systematically studied using molecular dynamics simulations. Specifically, interactions between screw dislocations and 60° mixed dislocations with both coherent and incoherent twin boundaries are examined. Importantly, the study considers both metastable and minimum-energy configurations of these twin boundaries to explore the impact of local atomic arrangements on dislocation-twin boundary interactions. The results indeed reveal two distinct mechanisms for dislocation transmission through twin boundaries: partial dislocation reaction versus full dislocation absorption followed by emission in the adjacent grain. The observed interaction mechanisms are found to be similar in the case of other symmetric tilt GBs with similar local structural units. Therefore, the interplay between dislocation type and grain boundary (GB) structure can strongly influence the transmission of dislocations across GBs. Even a subtle change of approximately 1.5% in the nearest-neighbor distance of the coherent twin boundary (metastable vs minimum-energy structure) alters the outcome of the dislocation-twin boundary interaction (transmission vs absorption). Specifically, the screw dislocation can transmit through metastable but not the minimum-energy coherent twin boundary. This further highlights the important role of GB structure, especially those metastable structures, in material strength modeling.

DOI: [10.1103/PhysRevMaterials.8.063604](https://doi.org/10.1103/PhysRevMaterials.8.063604)

## I. INTRODUCTION

The interactions between dislocations and grain boundaries (GBs) greatly influence the mechanical strength of a material [1,2]. Macroscopically, the effects of this interaction can be captured by using simple grain-boundary strengthening models (Hall-Petch relationship), where the strength of a material can be modulated by the average grain size [3]. While these models predominantly take grain size into account, with some possible consideration of misorientation, there are no parameters in the models to define the role of GB structure. The nature of dislocation-GB interaction (DGI) and its dependence on GB structure is not well-understood despite multiple experimental, theoretical, and computational efforts over the past few decades [4–8]. Experimentally, motivated by slip system geometry and/or internal stresses, there have been several proposed criteria for dislocation transmission based on a geometry-based approach (N criterion), combined geometry- and stress-based approach (M criterion), and GB structure (consideration of residual Burgers vector) [5]. However, these criteria fail to capture the effect of local atomic environment of the GBs on DGI.

There have been a few efforts to consider the effect of local atomic environment on DGIs [4–8]. Atomistic simulations are ideally suited for investigating the effect of local atomic environments by assessing the isolated DGI over a wide variety of material systems, grain boundary structures,

and dislocation types [4,5]. Early atomistic works by Dewald *et al.* [6,7] and Bachurin *et al.* [8] revealed the influence of dislocation types (edge, screw, or mixed) and grain boundary structures (specific locations of the interaction points) on the outcome of DGI in Ni and Al. Given the broad space of possible DGI, a common strategy is to simplify the problems by choosing a specific type of dislocation or grain boundary structure to investigate. Among those grain boundaries, coherent and incoherent twin boundaries (TBs) are often chosen as prototypes due to their simple structures and important role in deformation [9–13]. Jin *et al.* [9] and Chassagne *et al.* [11] found a correlation between the stacking fault energies and the outcome of the screw dislocation; coherent twin boundary interaction for different FCC metals. Additionally, Ma *et al.* [13] demonstrated that the stress for dislocation transmission can vary depending on the interaction sites for screw dislocation interaction with an incoherent TB in Cu. In parallel, Ezez *et al.* [12] suggested that the DGI results can be significantly different depending on the type of dislocations that nucleate from a preexisting void. For the incoherent TB in Ni, Liang *et al.* found that incoming screw dislocations can cross-slip onto incoherent twin boundaries (ITB) and push out the ITB interface dislocation due to a repulsive force between the two dislocations. On the other hand, a mixed dislocation can only transmit through the ITB if the leading partial reacts with interface dislocation to produce a full dislocation [14].

Despite the above work, there is still no comprehensive study on DGI depending on dislocation type and GB structure. Specifically, previous studies have either (1) focused on only one dislocation type and/or (2) were not performed under a

\*Contact author: kq dang@lanl.gov

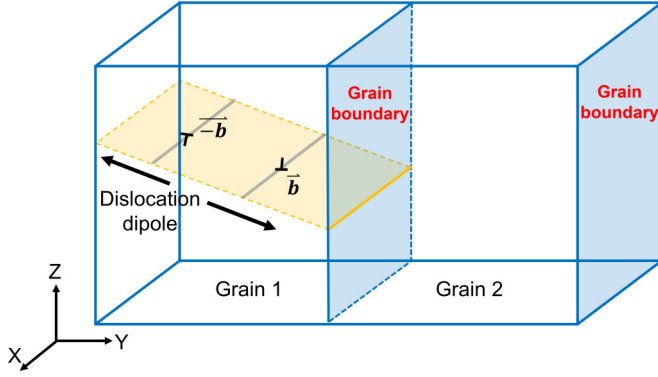


FIG. 1. Simulation setup with a bicrystal composed of two symmetric  $\langle 110 \rangle$  tilt GBs. An infinitely long dislocation dipole with screw and mixed ( $60^\circ$ ) character angles is generated in grain 1 using a dislocation loop algorithm developed by Dang *et al.* [24,25] (inspired by Ref. [19]). (Disclaimer: the dimensions of the schematics are not scaled with the dimensions used in this work.)

well-defined stress state. Moreover, metastable (also referred to as nonequilibrium) GB structures were commonly observed in previous experimental characterization of microstructures [15]. However, so far, only minimum-energy/equilibrium (the lowest energy) GB configurations have been considered in previous DGI studies [6–13]. Therefore, the goal of this work is to demonstrate the role of metastable GBs on the DGIs and eventually the importance of incorporating realistic metastable GB structures in material strength modeling. Here, coherent and incoherent TBs are focused due to their frequent observation in microstructure and their important role in deformation [9–13].  $60^\circ$  mixed and screw dislocations are chosen to ensure that the same state of stress (pure shear stress in the slip direction) can be enforced for each simulation run.

Thus, this work systematically investigates the interactions between  $60^\circ$  mixed and screw dislocations with metastable and minimum-energy configurations of the coherent and incoherent twin boundaries in Cu using MD simulations. This work discovers two different local interaction mechanisms for the full transmission of  $60^\circ$  mixed and screw dislocations through the TBs, which also apply to other  $\langle 110 \rangle$  symmetric tilt GBs in the same family. Importantly, the metastable structures of the coherent twin boundary (CTB) can greatly influence the outcome of DGI.

## II. SIMULATION METHODS

Figure 1 shows the bicrystal with a symmetric  $\langle 110 \rangle$  tilt GB utilized in this work. The construction of this bicrystal follows the standard  $\gamma$ -surface approach [16,17]. Here, the X direction is always oriented along the  $[\bar{1}\bar{1}0]$  tilt axes and the Y direction is normal to the GB plane (which can be found in Ref. [16] for all GB structures described in Table I). Periodic boundary conditions are employed in all three directions to allow for complete control of the stress state. This simulation setup has been demonstrated to be efficient and appropriate for DGI in previous work [18]. Boundary image forces can influence the outcome of DGI. Thus, the simulation cell has to be large enough to minimize this effect on the

TABLE I. List of selected Cu GBs along with the corresponding coincidence site lattice (CSL) representation, calculated GB energy ( $\gamma_{GB}$ ), and GB-dislocation interaction outcome. For  $\Sigma 3(1\ 1\ 2)$ , there are three interaction sites (denoted by \*, \*\*, and \*\*\*) corresponding to the location of an edge partial,  $30^\circ$  partial, and  $60^\circ$  partial, respectively. T = full transmission, PT = partial transmission, A = absorption, and P = pinned at the pinned at the grain boundaries.

$\theta$ ( $^\circ$ )	CSL	$\gamma_{GB}$ (mJ/m $^2$ )	GB-dislocation Interaction Outcome	
			Mixed	Screw
55.88	$\Sigma 41(3\ 3\ 8)$	577	T	A
55.88	$\Sigma 41(3\ 3\ 8)$	671	T	A
55.88	$\Sigma 41(3\ 3\ 8)$	693	T	A
59.0	$\Sigma 33(2\ 2\ 5)$	592	T	A
59.0	$\Sigma 33(2\ 2\ 5)$	701	T	A
70.5*	$\Sigma 3(1\ 1\ 2)$	601	T	A
70.5**	$\Sigma 3(1\ 1\ 2)$	601	PT	PT
70.5***	$\Sigma 3(1\ 1\ 2)$	601	PT	PT
70.5*	$\Sigma 3(1\ 1\ 2)$	660	T	A
70.5**	$\Sigma 3(1\ 1\ 2)$	660	PT	PT
70.5***	$\Sigma 3(1\ 1\ 2)$	660	PT	PT
109.5	$\Sigma 3(1\ 1\ 1)$	22	P	A
109.5	$\Sigma 3(1\ 1\ 1)$	113	P	T
109.5	$\Sigma 3(1\ 1\ 1)$	174	P	T
119.0	$\Sigma 97(6\ 6\ 5)$	516	P	T

reactions. The simulation cell contains about 400,000 atoms and is approximately  $1.0 \times 100.0 \times 48.0\text{nm}^3$  in the X, Y, and Z directions, respectively. This size was found to minimize the effects of periodic boundary conditions on the simulation results [18]. In addition to the coherent and incoherent TB, symmetric tilt GBs with similar structural units (defined by Rittner *et al.* in Ref. [19]) are also considered (see Table I). To determine the structure of the tilt boundaries, different starting configurations are considered by translating grain 2 relative to grain 1 (see Fig. 1) and selecting the configuration that minimizes the total energy (denoted as the minimum-energy structure) as well as those with higher energies corresponding to the metastable structures. The initial GB energy for each GB considered in this work is provided in Table I. The defect energies ( $E_d$ ) (dislocation and GB energy) are also tracked during the interaction by subtracting the total energy around the GB region (8 nm region around the GB) by the corresponding cohesive energy under the same loading and temperature condition and normalized by the dislocation line length.

The embedded atom model (EAM) potential developed by Mishin *et al.* [20] for Cu is used since it can accurately reproduce both GB and dislocation properties such as GB structures and dislocation core structures [21]. This potential has also been widely used to study DGI in FCC systems [9,11,13]. All molecular dynamics (MD) simulations are performed using the classical molecular dynamics code Large-scale Atomic/Molecular Massively Parallel Simulator (LAMMPS) [22] and the results are analyzed using the Open Visualization Tool (OVITO) [23].

To model DGIs, an infinitely long dislocation dipole with screw and mixed ( $60^\circ$ ) character angles is generated in grain

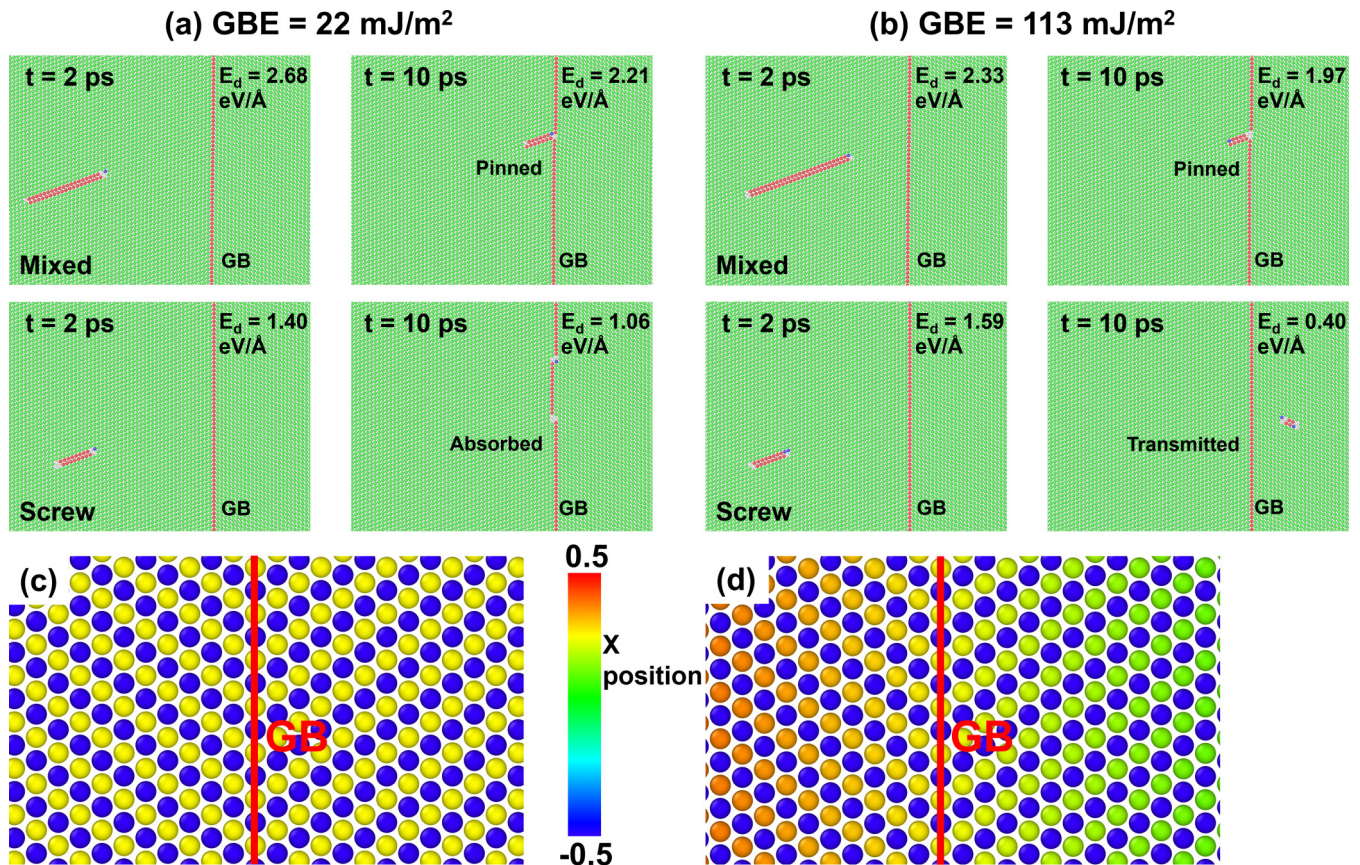


FIG. 2. Snapshots of the interactions between screw and mixed dislocations with (a) minimum-energy and (b) metastable coherent twin boundaries ( $\Sigma 3 \{111\}$ ) at the beginning (2 ps) and after (10 ps). Atoms are colored by structure types (red atoms are HCP and green atoms are FCC). (c) and (d) show the initial structures of minimum-energy and metastable coherent twin boundaries, respectively. Here, atoms are colored by their X positions (along the  $[\bar{1}\bar{1}0]$  direction) to show the 0.6% shear between the right and left grain. The red line marks the location of the coherent twin boundary. The defect energies at each time step are also shown at the top right corner of each subfigure.

1 using a dislocation loop algorithm developed by Dang *et al.* [24,25]. The dipole length is about 36 nm to minimize interactions between the dislocations. The chosen slip systems are  $[\bar{1}\bar{1}0](1\bar{1}\bar{1})$  and  $[01\bar{1}](1\bar{1}\bar{1})$  for screw and mixed dislocations, respectively. Here, only the interaction between the right dislocation of the dislocation dipole and the center GB is analyzed and reported. The dislocation dipole is positioned in a way that the right dislocation is approximately 8 nm away from the center of the GB region to minimize any short-range interactions initially. The system with the dislocation configuration is then equilibrated at 10 K via a Nosé-Hoover style thermostat and barostat [26].

For each case, a resolved shear stress (Schmid stress) of 500 MPa is applied to glide the dislocation toward the GB.

This corresponds to the stress state of  $\begin{bmatrix} 0 & -165 & 470 \\ -165 & 0 & 0 \\ 470 & 0 & 0 \end{bmatrix}$  MPa

and  $\begin{bmatrix} 235 & -135 & 335 \\ -135 & 80 & -195 \\ 335 & -195 & -315 \end{bmatrix}$  MPa for the screw and mixed dislocations interacting with the CTB, respectively. Similarly,

the corresponding stress states for the interactions between screw and mixed dislocations with the ITB are  $\begin{bmatrix} 0 & 0 & 500 \\ 0 & 0 & 0 \\ 500 & 0 & 0 \end{bmatrix}$

MPa and  $\begin{bmatrix} 0 & -250 & 433 \\ -250 & 0 & 0 \\ 433 & 0 & 0 \end{bmatrix}$  MPa, respectively. Since the ITB

structure contains three distinct partial dislocations [13,27,28] (as shown in Fig. S1), three different interaction sites (corresponding to the location of each partial dislocation) are considered in this work. Each simulation is repeated three times with different random initial atom velocities within a thermal distribution. The results (DGI outcome, local stress, and local energy structures) from these multiple sets of simulations are analyzed to see if they are statistically meaningful.

### III. RESULTS AND ANALYSIS

Figures 2(a) and 2(b) show the interaction between mixed and screw dislocations with the minimum-energy and metastable CTBs ( $\Sigma 3 \{111\}$ ), respectively. Two snapshots are provided for each case where the dislocation approaches the boundary at 2 ps and interacts with it at 10 ps. Before the interaction, both screw and mixed dislocations dissociate into two Shockley partials as is preferred for FCC system [29]. For screw and  $60^\circ$  mixed dislocations, the dissociation reactions are

$$\frac{a_o}{2}[\bar{1}\bar{1}0] \rightarrow \frac{a_o}{6}[\bar{1}\bar{2}1] + \frac{a_o}{6}[\bar{2}\bar{1}\bar{1}], \quad (1)$$

$$\frac{a_o}{2}[01\bar{1}] \rightarrow \frac{a_o}{6}[\bar{1}\bar{1}\bar{2}] + \frac{a_o}{6}[12\bar{1}], \quad (2)$$

where  $a_0$  is the lattice constant, which is 0.361 nm for Cu in this interatomic potential. The equilibrium distance of the screw dislocation is 1 nm and of mixed dislocation is 2.5 nm, which is consistent with a previous study [9]. As the dislocation approaches and touches the grain boundaries, the separation distance between the two partials is shortened as shown in Fig. 2(a). For both minimum-energy and metastable coherent TBs, the mixed dislocation gets pinned at the GBs. In contrast, the screw dislocation gets absorbed into the minimum-energy CTB structure but transmits through the metastable CTB. The former is in agreement with previous interaction results corresponding to the driving stress of 500 MPa from both modeling using the same interatomic potentials [9,11] and experiments where the coherent TB can absorb the dislocation, thus providing resistance to slip transmission [11]. On the other hand, the latter demonstrates that once perturbed, imperfect or metastable coherent TBs (with only 0.6% macroscopic shear strain along the tilt axis ( $[\bar{1}\bar{1}0]$  direction), see Figs. 2(c) and 2(d), can alter the DGI outcome from absorption to transmission.

The differences between these interactions can be rationalized by the varying local atomic arrangements at the GB. Before loading, there is a 0.6% macroscopic shear strain along the tilt axis ( $[\bar{1}\bar{1}0]$  direction) between the right and left grain for the metastable structure instead of the mirror symmetry of the minimum-energy CTB [as shown in Figs. 2(c) and 2(d)]. This probably causes the shift in activation energies between the two processes (transmission vs absorption), which leads to transmission becoming more favorable. Figure 3 shows the local atomic structure (polyhedrons at GB) of both minimum-energy and metastable CTB during loading when screw dislocations interact with the CTB. These polyhedrons, which describe the local atomic structure at GB, are identified using graph theory via the NETWORKX package [30], wherein pairwise distances are measured through a quick nearest-neighbor lookup utilizing the SCIPY KDTree package [31], applying a cutoff of 4.299 Å. For in-depth analysis, two neighboring polyhedrons at the GB-dislocation interaction site are selected, and their evolution over time is examined. These polyhedrons, henceforth termed structural units (SUs), are formed using five interconnected nodes, where the central layer consists of a twin or HCP atom, and the top and bottom layers are comprised of FCC atoms prior to interaction, as shown in Fig. 3(a). Figure 3(a) also shows a heatmap of the pairwise distances between nodes for the minimum-energy CTB at 0 ps. Further, the distance heatmap for minimum-energy CTB just before dislocation-GB interaction (at 3 ps) shows a modification in SUs. It highlights that the distance between vertically aligned FCC atoms (nodes: 1 & 2 and 8 & 9) remains unchanged, while the spacing between in-plane HCP atoms (nodes: 3 & 5 and 5 & 7) expands, signifying the elongation of SUs along the Z direction. Additionally, altered distances between HCP and FCC atoms suggest a minor in-plane rotation of HCP atoms. On the other hand, in metastable configurations [Figs. 3(b) and S2] the 3 ps SUs are different from the SUs in minimum-energy CTB at same time step (3 ps). In addition, there is a notable shift in the distance between vertically aligned FCC atoms (nodes: 1 & 2 and 8 & 9). This points to the compression of SUs along the vertical (Y) direction in metastable structures, altering the

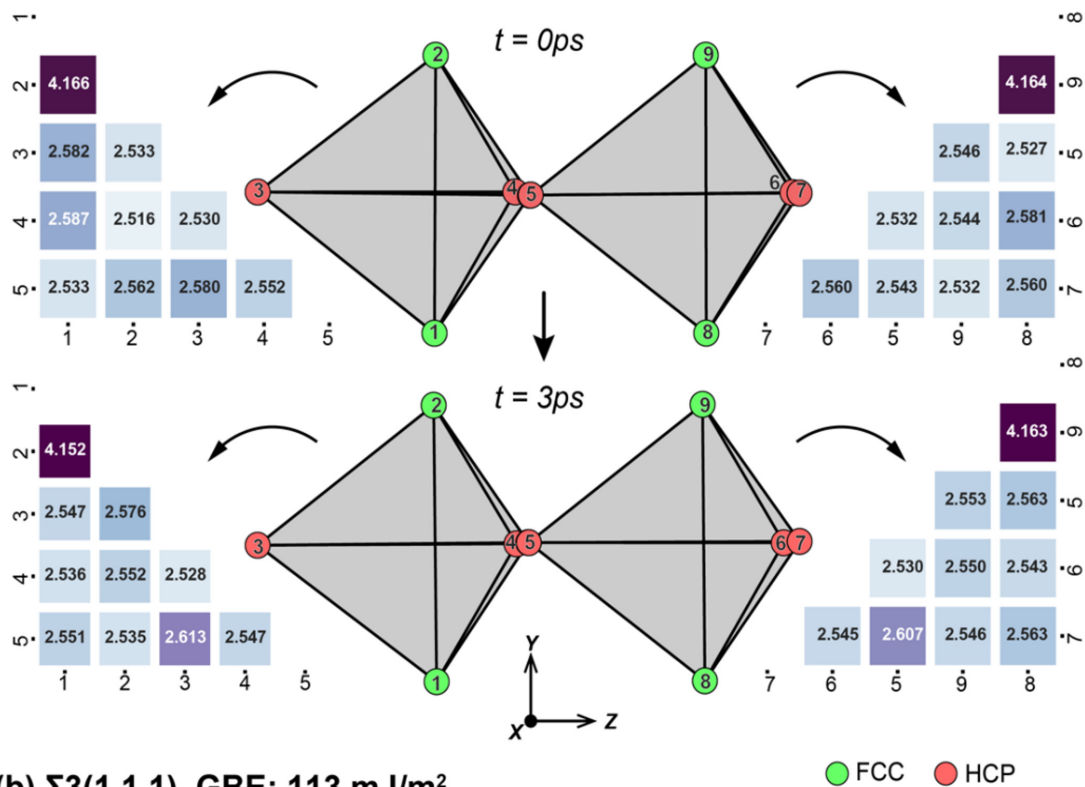
interlayer spacing between grains. Consequently, the in-plane deformation of SUs in minimum-energy CTB contributes to the absorption of screw dislocation at GB, whereas the out-of-plane deformation in metastable structures facilitates dislocation transmission across GB. These changes are small, amounting to a strain of  $\sim 1.5\%$  between the 3 ps structures of minimum-energy and metastable CTBs, given the minimal alterations in distance. These results raise the question of whether small differences in atomic structures between minimum-energy and metastable CTBs can lead to varying interactions between a screw dislocation and a CTB.

The absorption or transmission of a screw dislocation, when it interacts with the CTB, involves two processes. First, the dissociated dislocation is constricted back to a full dislocation (similar to the Friedel-Escaig mechanism for cross-slip) [32] under high enough applied stress (at least 400 MPa). Second, the compact dislocation is dissociated back into two partials to transmit into the neighboring grain [9,11]. The absorption of screw dislocation into the CTB is possible since the one-layer thick twinning disconnection mode has a Burgers vector exactly equal to the Shockley partials [33,34]. This competition between these two outcomes depends on the activation energy of each process, which is influenced by the structure of the CTBs.

For minimum-energy CTB, absorption is observed since it has lower activation energy compared to transmission as shown by previous MD simulations and nudged elastic band calculations [10,11,32]. Indeed, previous theoretical and modeling work by Chen *et al.* has shown that the difference in the activation energy of these two reactions (absorption vs transmission) is relatively small (0.342 eV/Å for absorption and cross-slip along the GB and 0.356 eV/Å for slip transmission) [10]. Assuming the same prefactors, a 4% difference in the activation energies translates to roughly a 5% difference in the rates when thermal fluctuations are large enough to result in the transition. This would imply that both reactions would be somewhat equally probable in a statistical sampling of screw dislocation; coherent twin boundary interaction. Furthermore, Chen *et al.* suggested that the outcome can be further influenced by thermal activations and strain rate effects [10]. The results in this study for metastable CTB where the screw dislocation prefers to transmit further indicate that the local atomic arrangement of the boundaries (even though small as demonstrated in the previous section) has modified the activation energies for absorption and transmission, which leads to one reaction becoming substantially more probable than the other one. Each simulation in this work has been repeated three times with different initial velocity conditions to assess the role of thermal-statistical sampling on the results. However, the outcome for each reaction remains the same, which could be due to the limited statistics and low simulation temperature (10 K).

On the other hand, the  $60^\circ$  mixed dislocation cannot constrict back to a full dislocation and its Burgers vector is not one of the twinning disconnection modes on the CTB. Therefore, it gets pinned at the CTB for both minimum-energy and metastable structures. These results show that metastable structures of GBs need to be considered in material strength modeling to comprehensively account for the effects of microstructure.

(a)  $\Sigma 3(111)$ , GBE: 22 mJ/m<sup>2</sup>



(b)  $\Sigma 3(111)$ , GBE: 113 mJ/m<sup>2</sup>

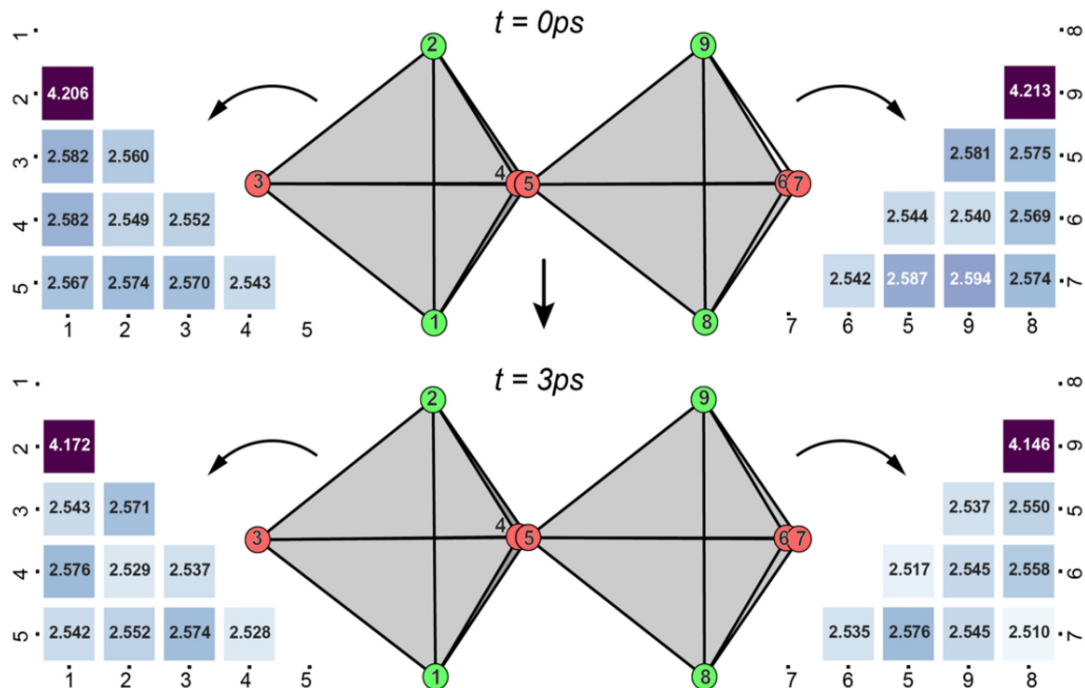


FIG. 3. Structural units identified using graph theory and corresponding distance heat map at the dislocation-GB interaction site for (a) minimum-energy (GBE: 22 mJ/m<sup>2</sup>) and (b) metastable (GBE: 113 mJ/m<sup>2</sup>) coherent twin boundaries ( $\Sigma 3 \{111\}$ ) at 0 ps and 3 ps (just before GB dislocation interaction). All the distances in the heatmap are in Å, and the numbers in the structural unit and the label of the heatmap represent nodes (arbitrary values). The “BuPu” colormap is used for the distance heatmap with lower and upper limits of 2.5 and 2.7 Å, respectively. (Note that Fig. 3 view is a 90° rotation of the view in Fig. 1 to analyze the structural units composed of the grain boundaries.)

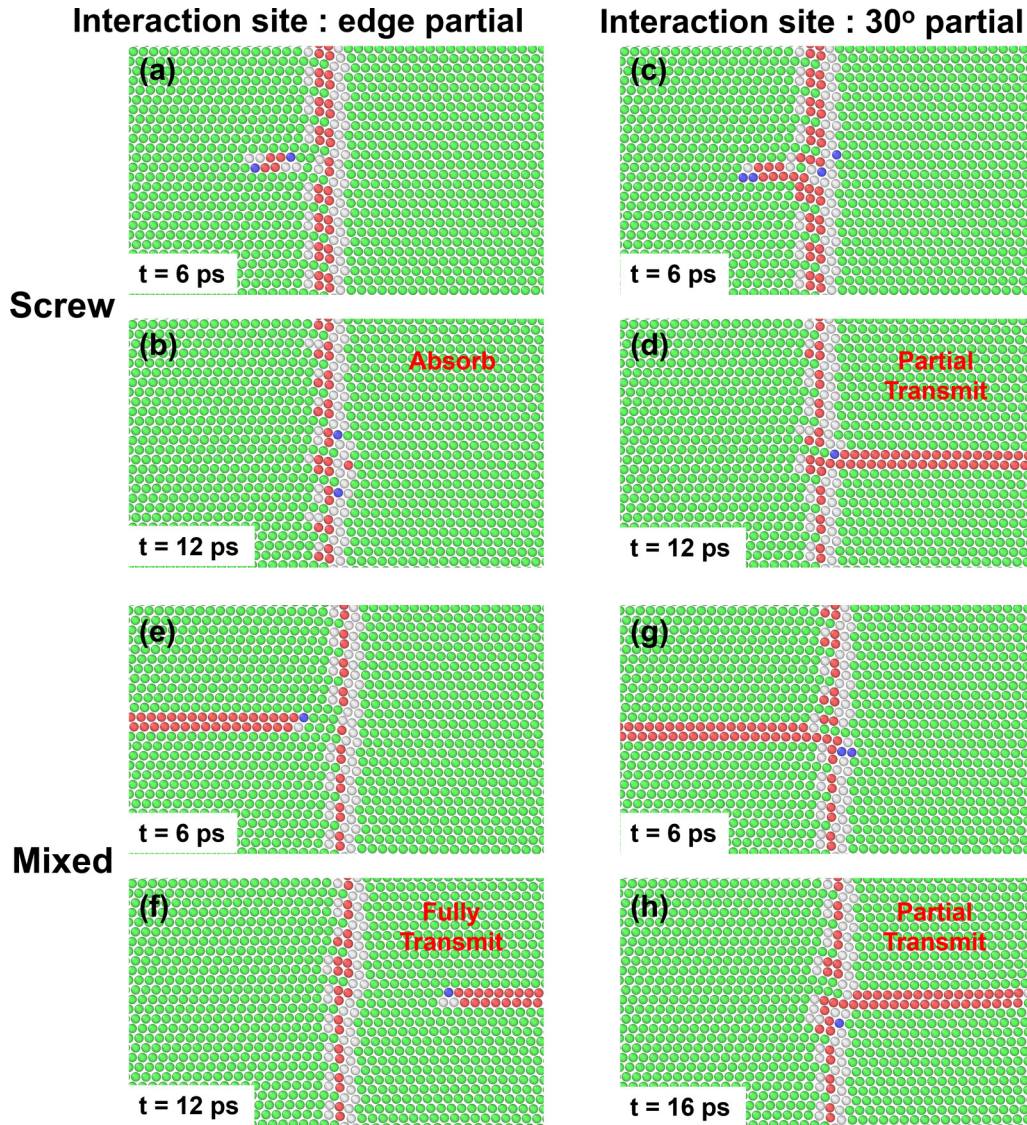


FIG. 4. Snapshots of the interactions between dislocations with the minimum-energy ITB ( $\Sigma 3 \{1\ 1\ 2\}$ ). (a), (b), (c), and (d) Interactions with screw dislocations at two different interaction sites (a), (c) before interaction (at  $t = 6\text{ps}$ ) and (b), (d) after interaction (at  $t = 12\text{ps}$ ). (e), (f), (g), and (h) Interactions with mixed dislocations at two different interaction sites (e), (g) before interaction (at  $t = 6\text{ps}$ ) and (f), (h) after interaction (at  $t = 12\text{ps}$  and  $t = 16\text{ps}$ , respectively). Atoms are colored by atom types (red are HCP atoms, green are FCC atoms, blue are BCC atoms, and white are undefined atoms). The figures on the right have interaction sites 1 atomic plane below the ones on the left.

Figure 4 shows the interaction between  $60^\circ$  mixed and screw dislocations with the minimum-energy ITB ( $\Sigma 3 \{1\ 1\ 2\}$ ) (with  $E_{GB} = 601\text{ mJ/m}^2$ ) for interaction sites aligned with the location of an edge partial and  $30^\circ$  partial on the ITB. Note that the interaction results for the site aligning with the  $60^\circ$  partial are similar to the ones with the  $30^\circ$  partial as shown in Table I. Figure 4 shows that the interactions are not only sensitive to the dislocation character angles (screw versus  $60^\circ$  mixed) but also the location of the interaction sites along the GBs. Among those four interactions shown in Fig. 4, only interaction between a screw dislocation with the edge partial site at ITB leads to dislocation absorption [see Figs. 4(a) and 4(b)]. The other three cases all result in dislocation transmission. Among those three, only  $60^\circ$  mixed dislocation interactions at the edge partial site on the ITB lead to complete transmission

as shown in Figs. 4(e) and 4(f). The transmission shears the top part of the grain boundary compared to the lower part but does not change the local structure of the TB. The dislocation analysis also shows that the transmitted dislocation (edge is the leading partial) is reversed compared to the incoming dislocation ( $30^\circ$  mixed is the leading partial). For the other two cases, only the leading edge partial is transmitted to the other grain, while the trailing partial is pinned by the ITB.

These results are consistent with results from previous MD simulations in Ni [14], which indicates that the outcome of the dislocation-ITB reaction is not as sensitive to stacking fault energies, dislocation core length (that is material systems or interatomic potentials) compared to the dislocation-CTB reaction. On the other hand, for dislocation-CTB reaction, both reaction mechanism and stress depend strongly on both

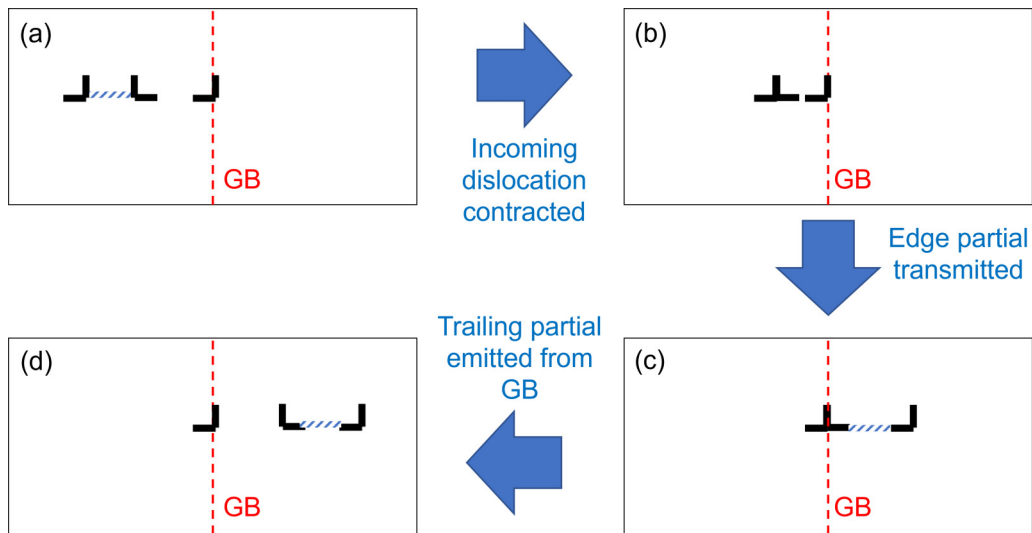


FIG. 5. Schematics of a possible sequence of events when a  $60^\circ$  mixed dislocation interacts with the minimum-energy incoherent TB ( $\Sigma 3 \{1\ 1\ 2\}$ ) at the edge partial site.

material systems and utilized interatomic potential [11]. Importantly, for the metastable structure (with slightly higher GB energy of  $E_{GB} = 660 \text{ mJ/m}^2$ ) of the ITB, these results remain the same. While the metastable ITB has slightly different atomic GB structure compared to the minimum-energy ITB, the structure composition of three partial dislocations remains the same. Together, these results indicate that the nature of the dislocation-ITB reaction is different from the dislocation-CTB interaction. The former can be treated as dislocation interactions where the dislocation Burgers vectors of the incoming dislocations and partial dislocations of the ITB dictate the outcome of the reaction. In this case, the DGI is insensitive to minor changes in the GB. On the other hand, the dislocation-CTB interaction is extremely sensitive to the geometric changes of the GB where even small changes (0.6% macroscopic shear strain and 1.5% in the nearest-neighbor distance of the coherent twin boundary) in the GB structure can result in a different outcome of DGI.

Figure 5 demonstrates a possible local dislocation reaction mechanism when a  $60^\circ$  mixed dislocation interacts with the minimum-energy ITB ( $\Sigma 3 \{112\}$ ) at the edge partial ( $\frac{a_0}{6} [112]$ ) site (see Video S3 in the Supplemental Material [35]). As the dislocation comes close to the TB, the leading  $30^\circ$  partial is slowed down by the repulsive force from the partial dislocations within the ITB, while the trailing edge partial still moves. Therefore, the stacking fault width of the incoming dislocation reduces significantly (from 7.7 nm to 3 nm) as shown in the Video S3 in the Supplemental Material [35]. As the driving force increases, the compacted incoming dislocation exerts a repulsive force on the partial dislocations within the TB. As a result, the edge partial dislocation from the ITB is emitted to the neighboring grain [see Fig. 5(c)]. Once emitted, the edge partial glides away from the ITB, increasing the stacking fault width, which exerts an attractive force on the incoming compacted dislocation. Once the stacking fault width reaches a critical length, the incoming dislocation dissociates again and its  $30^\circ$  leading partial glide away from the ITB and combines with the already transmitted edge partial to form a dissociated  $60^\circ$  mixed dislocation in the neighboring grain

as shown in Fig. 5(d). This potential local chain of events also helps to explain the other MD results for the ITB. When the interaction site is at either  $30^\circ$  or  $60^\circ$  mixed partials of the ITB, the outcome is partial transmission since the dissociated partials from the incoming dislocation cannot cross-slip and recombine with the edge leading partial of the ITB. On the other hand, for the screw dislocation with the interaction site at the edge partial of the ITB [Figs. 4(a) and 4(b)], the net Burgers vector between the screw dislocation and the edge partial within the ITB results in the formation of a  $30^\circ$  mixed partial within the ITB after the interaction. As a result, the screw dislocation is absorbed into the ITB at 500 MPa. At higher stresses, it has been shown that partial transmission can occur at this site [13].

While the mechanisms for the interactions between screw and mixed dislocations with either CTBs or ITBs are different, they both demonstrate the role of local boundary structure in the outcome of the DGIs. Importantly, these mechanisms are also pertinent to other  $\langle 110 \rangle$  symmetric tilt grain boundaries (STGBs) which share similar local structures as the incoherent and coherent TBs [19].

Figure 6 shows the full transmission of mixed and screw dislocations when interacting with  $\Sigma 41 \{3\ 3\ 8\}$ ,  $\Sigma 33 \{2\ 2\ 5\}$ , and  $\Sigma 97 \{6\ 6\ 5\}$  STGBs. The  $\Sigma 41 \{3\ 3\ 8\}$  and  $\Sigma 33 \{2\ 2\ 5\}$  share the edge partial structure of the GB similar to the one of the ITB and thus have the same full transmission outcome when interacting at a very similar site. On the other hand, the  $\Sigma 97 \{6\ 6\ 5\}$  STGB contains the straight coherent segment similar to the CTB and thus allows the full transmission of a screw dislocation, as in metastable CTB, when the interaction site is within that local coherent segment. We hypothesize that distortions in the coherent segment due to the presence of neighboring incoherent regions favor transmission over absorption. It could also be due to the inability of the twinning disconnection pair (the result of absorption into a CTB) to be sufficiently separated to reduce its energy. If the latter is true, the reaction might transition into absorption at a critical length of the coherent segment for this class of STGBs.

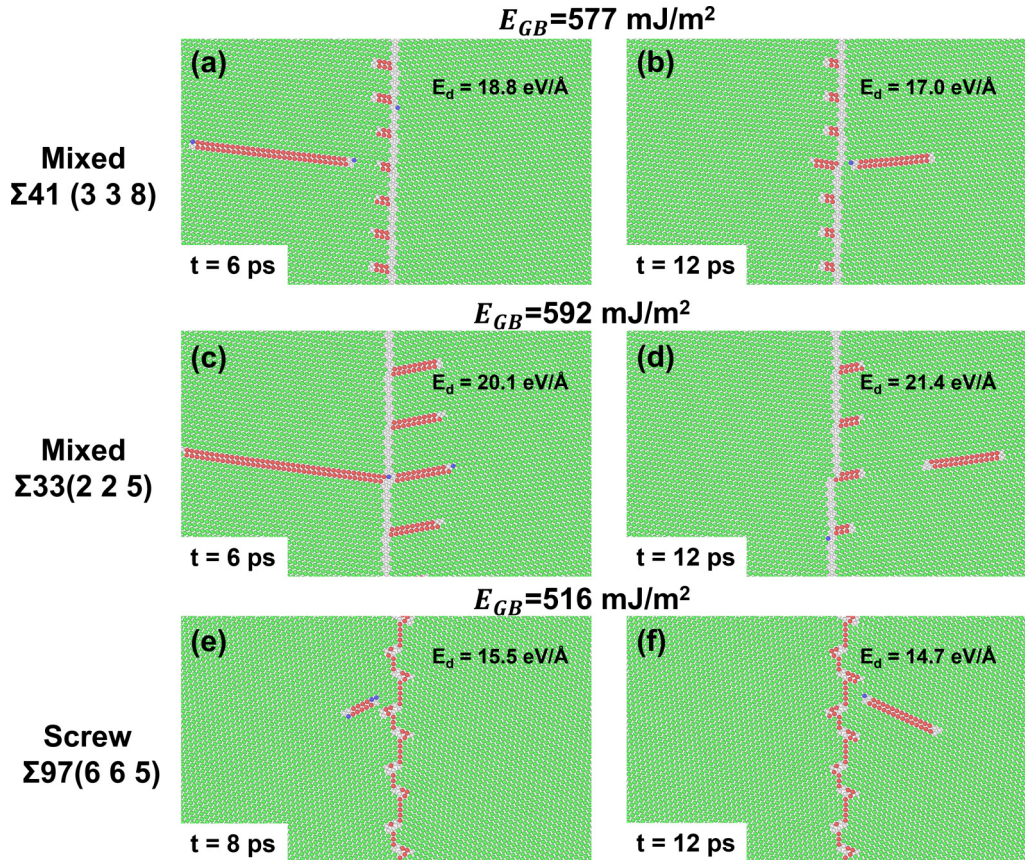


FIG. 6. Snapshots of the complete transmission when dislocations interact with different  $\langle 110 \rangle$  STGBs. Interactions between  $60^\circ$  mixed dislocation with  $\Sigma 41 \{3\ 3\ 8\}$  (a) before ( $t = 6$  ps) and (b) after interaction (at  $t = 12$  ps). Interactions between a  $60^\circ$  mixed dislocation with  $\Sigma 33 \{2\ 2\ 5\}$  (c) before ( $t = 6$  ps) and (d) after interaction (at  $t = 12$  ps). Interactions between a screw dislocation with  $\Sigma 97 \{6\ 6\ 5\}$  (e) before ( $t = 8$  ps) and (f) after interaction (at  $t = 12$  ps). Atoms are colored by atom types (red are HCP atoms, green are FCC atoms, blue are BCC atoms, and white are undefined atoms).

Atomistic results provide a mechanistic understanding of DGI at the atomic level to advance material strength modeling (at higher length scale). Specifically, atomistic details such as dislocation core structure, GB structure, and reaction outcome can be used to parameterize mesoscale modeling such as phase field or dislocation dynamics simulations. These mesoscale modeling techniques can model much larger material volumes and serve as a bridge between atomistic and macroscopic modeling techniques. For instance, a recent study of dislocation transmission across  $\Sigma 3\{112\}$  ITB using a combined approach atomistic and phase field (PF) has demonstrated how treatment of grain boundary as misfit dislocations in the PF can capture reasonable MD simulation results [13]. Importantly, results from this work demonstrate that local atomic configuration is essential to DGI for certain GB structures (CTB) but not others (ITB). For these structure-sensitive GBs, one needs to adopt different approaches (from the approach in Ref. [13]) to appropriately model DGI at the mesoscale level. One suggestion would be to use high-fidelity atomic environment descriptors (such as Spectral Neighbor Analysis Potential (SNAP) [36,37], Smooth Overlap of Atomic Positions (SOAP) [38,39], Atomic Cluster Expansion (ACE) [40], Strain Functional Descriptor (SFD) [41]) to describe DGI. Higher-order deformations, which result from the higher order gradients in the local number density, can be used

to describe minor changes to the GB during the interactions with dislocation (similar to the 1.5% change in local structure observed in this study).

#### IV. CONCLUSIONS

In conclusion, this systematic study on the effects of dislocation type and metastability of GB structures on the DGI outcomes has revealed two distinct interaction mechanisms between screw and mixed dislocations with coherent and incoherent twin boundaries. Screw dislocation can transmit through the CTB easier than the  $60^\circ$  mixed dislocation. It is also found that distortions to the CTB can also change the interaction from absorption to transmission. The difference in DGI outcomes for the ITB can be explained as a result of the interplay between dislocation type and local GB structure. Importantly, the observed mechanisms apply to other STGBs that share the same local boundary structure. This further demonstrates the importance of including metastability GB structures (with small locally altered structures) in mesoscale modeling to appropriately capture the DGI outcomes. Thus, understanding DGIs at the atomic scale, such as results from this work, becomes necessary for multiscale material strength modeling and motivates similar related studies in the future.

## ACKNOWLEDGMENTS

Research presented in this work was fully supported by the Laboratory Directed Research and Development program of Los Alamos National Laboratory, United States under Grant No. 20210036DR, “Investigating How Material’s Interfaces

and Dislocations Affect Strength” (iMIDAS). This research used resources provided by the Los Alamos National Laboratory Institutional Computing Program, which is supported by the U.S. Department of Energy National Nuclear Security Administration under Contract No. 89233218CNA000001.

- [1] J. Kacher, B. P. Eftink, B. Cui, and I. M. Robertson, Dislocation interactions with grain boundaries, *Curr. Opin. Solid State Mater. Sci.* **18**, 227 (2014).
- [2] H. Pan, Y. He, and X. Zhang, Interactions between dislocations and boundaries during deformation, *Materials (Basel)*. **14**, 1012 (2021).
- [3] N. Hansen, Hall-Petch relation and boundary strengthening, *Scr. Mater.* **51**, 801 (2004).
- [4] D. W. Adams, D. T. Fullwood, R. H. Wagoner, and E. R. Homer, Atomistic survey of grain boundary-dislocation interactions in FCC nickel, *Comput. Mater. Sci.* **164**, 171 (2019).
- [5] D. E. Spearot and M. D. Sangid, Insights on slip transmission at grain boundaries from atomistic simulations, *Curr. Opin. Solid State Mater. Sci.* **18**, 188 (2014).
- [6] M. P. Dewald and W. A. Curtin, Multiscale modelling of dislocation/grain-boundary interactions: I. Edge dislocations impinging on  $\Sigma 11$  (1 1 3) tilt boundary in Al, *Model. Simul. Mater. Sci. Eng.* **15**, S193 (2007).
- [7] M. P. Dewald and W. A. Curtin, Multiscale modelling of dislocation/grain boundary interactions. II. Screw dislocations impinging on tilt boundaries in Al, *Philos. Mag.* **87**, 4615 (2007).
- [8] D. V. Bachurin, D. Weygand, and P. Gumbsch, Dislocation-grain boundary interaction in (111) textured thin metal films, *Acta Mater.* **58**, 5232 (2010).
- [9] Z.-H. Jin, P. Gumbsch, E. Ma, K. Albe, K. Lu, H. Hahn, and H. Gleiter, The interaction mechanism of screw dislocations with coherent twin boundaries in different face-centred cubic metals, *Scr. Mater.* **54**, 1163 (2006).
- [10] Z. Chen, Z. Jin, and H. Gao, Repulsive force between screw dislocation and coherent twin boundary in aluminum and copper, *Phys. Rev. B*. **75**, 212104 (2007).
- [11] M. Chassigne, M. Legros, and D. Rodney, Atomic-scale simulation of screw dislocation/coherent twin boundary interaction in Al, Au, Cu and Ni, *Acta Mater.* **59**, 1456 (2011).
- [12] T. Ezaz, M. D. Sangid, and H. Sehitoglu, Energy barriers associated with slip-twin interactions, *Philos. Mag.* **91**, 1464 (2011).
- [13] T. Ma, H. Kim, N. Mathew, D. J. Luscher, L. Cao, and A. Hunter, Dislocation transmission across  $\Sigma 3\{112\}$  incoherent twin boundary: A combined atomistic and phase-field study, *Acta Mater.* **223**, 117447 (2022).
- [14] Y. Liang, X. Yang, M. Gong, G. Liu, Q. Liu, and J. Wang, Slip transmission for dislocations across incoherent twin boundary, *Scr. Mater.* **166**, 39 (2019).
- [15] H. Gleiter, On the structure of grain boundaries in metals, *Mater. Sci. Eng.* **52**, 91 (1982).
- [16] M. A. Tschopp, S. P. Coleman, and D. L. McDowell, Symmetric and asymmetric tilt grain boundary structure and energy in Cu and Al (and transferability to other fcc metals), *Integr. Mater. Manuf. Innov.* **4**, 176 (2015).
- [17] J. Chen and S. J. Fensin, Associating damage nucleation and distribution with grain boundary characteristics in Ta, *Scr. Mater.* **187**, 329 (2020).
- [18] S. Suresh, K. Dang, and S. J. Fensin, Sensitivity of dislocation-GB interactions to simulation setups in atomistic models, *Comput. Mater. Sci.* **221**, 112085 (2023).
- [19] J. D. Rittner and D. N. Seidman, (110) symmetric tilt grain-boundary structures in fcc metals with low stacking-fault energies, *Phys. Rev. B*. **54**, 6999 (1996).
- [20] Y. Mishin, M. J. Mehl, D. A. Papaconstantopoulos, A. F. Voter, and J. D. Kress, Structural stability and lattice defects in copper: Ab initio, tight-binding, and embedded-atom calculations, *Phys. Rev. B*. **63**, 224106 (2001).
- [21] J. Chen, K. Dang, H. T. Vo, P. Hosemann, and S. J. Fensin, Associating GB characteristics with its sink efficiency in absorbing Frank loops in Cu, *Scr. Mater.* **192**, 61 (2021).
- [22] S. Plimpton, Fast parallel algorithms for short-range molecular dynamics, *J. Comput. Phys.* **117**, 1 (1995).
- [23] A. Stukowski, Visualization and analysis of atomistic simulation data with OVITO—the Open Visualization Tool, *Model. Simul. Mater. Sci. Eng.* **18**, 015012 (2010).
- [24] K. Dang, L. Capolungo, and D. E. Spearot, Nanoscale dislocation shear loops at static equilibrium and finite temperature, *Model. Simul. Mater. Sci. Eng.* **25**, 085014 (2017).
- [25] K. Dang, D. Bamney, K. Bootsita, L. Capolungo, and D. E. Spearot, Mobility of dislocations in Aluminum: Faceting and asymmetry during nanoscale dislocation shear loop expansion, *Acta Mater.* **168**, 426 (2019).
- [26] S. Melchionna, G. Ciccotti, and B. Lee Holian, Hoover NPT dynamics for systems varying in shape and size, *Mol. Phys.* **78**, 533 (1993).
- [27] J. Wang, N. Li, and A. Misra, Structure and stability of  $\Sigma 3$  grain boundaries in face centered cubic metals, *Philos. Mag.* **93**, 315 (2013).
- [28] J. Wang, O. Anderoglu, J. P. Hirth, A. Misra, and X. Zhang, Dislocation structures of  $\Sigma 3\{112\}$  twin boundaries in face centered cubic metals, *Appl. Phys. Lett.* **95**, 021908 (2009).
- [29] H. Häkkinen, S. Mäkinen, and M. Manninen, Edge dislocations in fcc metals: Microscopic calculations of core structure and positron states in Al and Cu, *Phys. Rev. B*. **41**, 12441 (1990).
- [30] A. A. Hagberg, D. A. Schult, and P. J. Swart, Exploring network structure, dynamics, and function using NetworkX, in *Proceedings of the 7th Python in Science Conference (SciPy2008)*, edited by G. Varoquaux, T. Vaught, and J. Millman (2008), pp. 11–16.
- [31] P. Virtanen, R. Gommers, T. E. Oliphant, M. Haberland, T. Reddy, D. Cournapeau, E. Burovski, P. Peterson, W. Weckesser, J. Bright *et al.*, SciPy 1.0: Fundamental algorithms for scientific computing in Python, *Nat. Methods* **17**, 261 (2020).
- [32] T. Zhu, J. Li, A. Samanta, H. G. Kim, and S. Suresh, Interfacial plasticity governs strain rate sensitivity and ductility in

- nanostructured metals, *Proc. Natl. Acad. Sci. USA* **104**, 3031 (2007).
- [33] E. A. Marquis and D. L. Medlin, Structural duality of  $1/3\langle 111 \rangle$  twin-boundary disconnections, *Philos. Mag. Lett.* **85**, 387 (2005).
- [34] J. Han, S. L. Thomas, and D. J. Srolovitz, Grain-boundary kinetics: A unified approach, *Prog. Mater. Sci.* **98**, 386 (2018).
- [35] See Supplemental Material at <http://link.aps.org/supplemental/10.1103/PhysRevMaterials.8.063604> for the dichromatic pattern analysis of the ITB; structural analysis using graph theory and corresponding distance heat map at the dislocation-GB interaction site for metastable (GBE: 174 mJ/m<sup>2</sup>) coherent twin boundaries; and a movie of the interactions between a mixed dislocation with the equilibrium incoherent TB ( $\Sigma 3$  112) at the edge partial dislocation site.
- [36] A. P. Thompson, L. P. Swiler, C. R. Trott, S. M. Foiles, and G. J. Tucker, Spectral neighbor analysis method for automated generation of quantum-accurate interatomic potentials, *J. Comput. Phys.* **285**, 316 (2015).
- [37] M. A. Wood and A. P. Thompson, Extending the accuracy of the SNAP interatomic potential form, *J. Chem. Phys.* **148**, 241721 (2018).
- [38] A. P. Bartók, R. Kondor, and G. Csányi, On representing chemical environments, *Phys. Rev. B* **87**, 219902(E) (2013).
- [39] A. P. Bartók, R. Kondor, and G. Csányi, Publisher's Note: On representing chemical environments [Phys. Rev. B **87**, 184115 (2013)], *Phys. Rev. B* **87**, 219902(E) (2013).
- [40] R. Drautz, Atomic cluster expansion for accurate and transferable interatomic potentials, *Phys. Rev. B* **99**, 014104 (2019).
- [41] E. M. Kober, J. P. Tavenner, C. M. Adams, and N. Mathew, Strain functionals: A complete and symmetry-adapted set of descriptors to characterize atomistic configurations, [arXiv:2402.04191](https://arxiv.org/abs/2402.04191).